Journal of Medicinal Chemistry Article

J. Med. Chem. **2010,** *53,* 8059–8071 **8059**
DOI: 10.1021/jm100793t

Disulfide Cyclized Tripeptide Analogues of Angiotensin IV as Potent and Selective Inhibitors of Insulin-Regulated Aminopeptidase (IRAP)

Hanna Andersson,[†] Heidi Demaegdt,[‡] Georges Vauquelin,[‡] Gunnar Lindeberg,[†] Anders Karlén,[†] Mathias Hallberg,[§] Máté Erdélyi,[∥] and Anders Hallberg*,[†]

[†]*Department of Medicinal Chemistry, Uppsala University, Box 574, SE-751 23 Uppsala, Sweden,* [‡]*Department of Molecular and Biochemical Pharmacology, Vrije Universiteit Brussel, Pleinlaan 2, 1050 Brussels, Belgium,* [§]*Department of Pharmaceutical Biosciences, Uppsala University, Box 591, SE-751 24 Uppsala, Sweden, and* [∥]*Department of Chemistry, University of Gothenburg, SE-412 96 Göteborg, Sweden*

Received June 27, 2010

The insulin-regulated aminopeptidase (IRAP) localized in areas of the brain associated with memory and learning is emerging as a new promising therapeutic target for the treatment of memory dysfunctions. The angiotensin II metabolite angiotensin IV (Ang IV, Val[1]-Tyr[2]-Ile[3]-His[4]-Pro[5]-Phe[6]) binds with high affinity to IRAP and inhibits this aminopeptidase (K_i = 62.4 nM). Furthermore, Ang IV has been demonstrated to enhance cognition in animal models and is believed to play an important role in cognitive processes. It is herein reported that displacement of the C-terminal tripeptide His[4]-Pro[5]-Phe[6] with a phenylacetic acid functionality combined with a constrained macrocyclic system in the N-terminal affords potent IRAP inhibitors that are less peptidic in character than the hexapeptide Ang IV. Configurational analysis of three pairs of diastereomeric Ang IV analogues was performed using a combination of solution NMR spectroscopic methods, Monte Carlo conformational searches, and NAMFIS calculations. The compounds encompassing L-amino acids only (**4**, **8**, and **12**) showed significantly higher bioactivity compared to their LLD-epimers (**5**, **9**, and **13**). The best inhibitors in the series, compounds **8** and **12**, incorporating a 13- and 14-membered disulfide ring system, respectively, and both with a β^3-homotyrosine residue (β^3hTyr) replacing Tyr[2], exhibit K_i values of 3.3 and 5.2 nM, respectively.

Introduction

There is an emerging demand for new drugs for the treatment of the cognitive decline associated with Alzheimer's disease as well as pathological conditions such as brain trauma and cerebral ischemia. Alzheimer's disease and other age-related neurological diseases are expected to be even more prevalent in the future with the increasing age of the population in most developed countries.[1,2] Apart from an NMDA antagonist,[3] all cognitive enhancers are cholinesterase inhibitors that prevent the degradation of acetylcholine. It is well-established that the cholinergic system is associated with learning and memory and that patients with Alzheimer's disease suffer from degradation of the cholinergic neurons in the brain. Unfortunately, neither the outcome of clinical studies on cholinesterase inhibitors and NMDA antagonists[4−7] nor those on nerve growth factors[8] and antioxidants[9−11] are encouraging. Today, considerable effort is devoted to studying interference with the amyloid-β processing enzymes and Aβ aggregation/oligomerization, as well as the tau protein, various kinases, and the 5-HT$_6$ receptor.[12−14] New avenues must be explored in order to enable the development of significantly improved cognitive enhancers. Recently published clinical data revealed that antihypertensives targeting the renin−angiotensin system (RAS[a]) induce beneficial effects in patients suffering from cognitive impairment.[15] On the basis of these clinical data and a large number of studies in animal models, the first report disclosed already in 1988,[16,17] it now seems clear that the angiotensin II metabolite angiotensin IV (**1**, Ang IV) plays an important role in cognitive processes. Thus, the receptor for the hexapeptide Ang IV (Val[1]-Tyr[2]-Ile[3]-His[4]-Pro[5]-Phe[6]) is emerging as a new promising therapeutic target, and selective interaction with this peptide receptor should provide a new approach for the treatment of memory dysfunctions.[15,18,19] Ang IV binds with high affinity to the insulin-regulated aminopeptidase (IRAP, EC 3.4.11.3)[20] localized in areas of the brain associated with memory and learning.[21−23] IRAP is a type II transmembrane protein that belongs to the same family of aminopeptidases as aminopeptidase N (AP-N)[24] and is often colocalized with the insulin-responsive glucose transporter GLUT4.[25]

Recently, Lukaszuk et al. reported several potent, selective, and stable analogues of Ang IV,[26,27] here exemplified by **AL-40** (Figure 1)[26] where Val[1] was substituted for β^2-homovaline

*To whom correspondence should be addressed. Phone: +46 18 471 4284. Fax: +46 18 4714474. E-mail: Anders.Hallberg@orgfarm.uu.se.

[a] Abbreviations: Aia, 4-amino-1,2,4,5-tetrahydroindolo[2,3-*c*]azepin-3-one; AMPA, 2-(aminomethyl)phenylacetic acid; Ang IV, angiotensin IV; AP-N, aminopeptidase N; Bn, benzyl; DIC, *N*,*N*′-diisopropylcarbodiimide; DIEA, *N*,*N*-diisopropylethylamine; DTT, threo-1,4-dimercaptobutane-2,3-diol; EDTA, 2-[2-[bis(carboxymethyl)amino]ethyl(carboxymethyl)amino]acetic acid; Fmoc, 9-fluorenylmethoxycarbonyl; methylindole AM resin, [3-((methyl-Fmoc-amino)methyl)indol-1-yl]acetylaminomethyl resin; FMPB AM resin, 4-(4-formyl-3-methoxyphenoxy)-butyrylaminomethyl resin; HATU, 1-[bis(dimethylamino)methyliumyl]-1*H*-1,2,3-triazolo[4,5-*b*]pyridine-3-oxide hexafluorophosphate; HBTU, 3-[bis(dimethylamino)methyliumyl]-3*H*-benzotriazol-1-oxide hexafluorophosphate; Hcy, homocysteine; HOBt, 1-hydroxybenzotriazole; β^3hTyr, β^3-homotyrosine; IRAP, insulin-regulated aminopeptidase; NAMFIS, NMR analysis of molecular flexibility in solution; RAS, renin−angiotensin system; ^{t}Bu, *tert*-butyl; TES, triethylsilane; TFA, trifluoroacetic acid; TMP, 2,4,6-trimethylpyridine; Trt, trityl.

Published on Web 11/03/2010

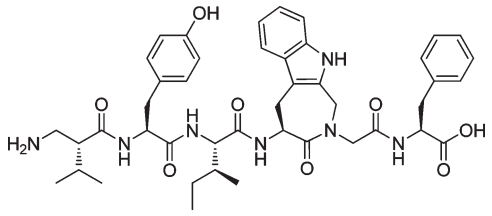

AL-40, K_i = 8.5 nM

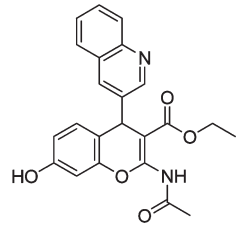

HFI-437, K_i = 20 nM

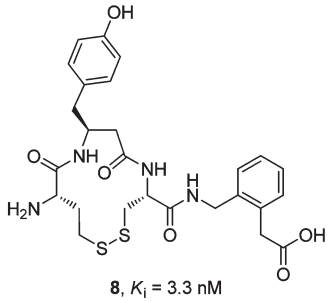

8, K_i = 3.3 nM

Figure 1. Previously reported IRAP inhibitors **AL-40**[26] and **HFI-437**[28] together with a novel inhibitor discussed in this paper.

(β^2hVal) and the His^4-Pro^5 dipeptide was replaced by 4-amino-1,2,4,5-tetrahydroindolo[2,3-*c*]azepin-3-one (Aia)-Gly. In 2008, a major step toward bioavailable IRAP inhibitors was taken by Albiston et al.[28] A series of potent druglike IRAP inhibitors, exemplified by **HFI-437** (Figure 1), were identified by the Australian group utilizing homology modeling of the catalytic domain of the protein and in silico screening methodologies. It was demonstrated in rat that the performance in both spatial working and recognition memory paradigms could be improved after administration of the inhibitor into the lateral ventricles.[28] We have applied the opposite strategy, which relies on introducing conformational constraints in Ang IV as the first objective.[29−31] Subsequent iterative structural modifications are expected to provide bioavailable nonpeptidic inhibitors with enhanced selectivity. We here show that cyclization of the N-terminal end of Ang IV truncated in the C-terminal can provide potent IRAP inhibitors that do not interfere with AP-N, as exemplified by compound **8** (Figure 1).

Results and Discussion

Chemistry. The syntheses of **2** and **3** have been reported previously.[31] Compounds **4**−**13** in Table 1 were prepared by manual SPPS using the Fmoc protection strategy[32] followed by oxidative cyclization in solution according to the synthetic routes outlined in Schemes 1−3.

Generally, the amino acids were single-coupled using HATU and DIEA in DMF. Under these conditions cysteine is prone to racemization. Consequently, the coupling reagent, base, and solvents must be chosen carefully.[33] Here, HATU, TMP, and CH_2Cl_2/DMF, with a minimum of DMF, were used in the majority of couplings. This method was also frequently applied for coupling of homocystein (Hcy). Fmoc deprotection was accomplished using 20% piperidine in DMF. Completeness of the coupling reactions was usually confirmed by small scale cleavage and LC−MS analysis. The coupling−deprotection cycle was repeated until the desired amino acid sequence had been synthesized. TFA/H_2O in the presence of TES and DTT was used to deprotect and cleave the intermediates from the solid supports. The scavenger DTT was used to prevent the *tert*-butyl (^{t}Bu) cations from reacting with the free thiol groups of the cysteine and homocysteine residues. After purification by RP-HPLC, the linear intermediates were subjected to disulfide cyclization in DMSO/TFA.[34−36] Finally, the cyclic Ang IV analogues were purified by preparative RP-HPLC and isolated as the corresponding TFA salts by lyophilization.

Analogues **4**, **5**, **8**, **9**, **12**, and **13** (Scheme 1) were synthesized by initial attachment of 2-(azidomethyl)phenylacetic acid[29] to 2-chlorotrityl chloride resin. Subsequently, the *S*-trityl protected Fmoc-Cys(Trt)-OH or Fmoc-Hcy(Trt)-OH was coupled via a Staudinger/aza-Wittig reaction.[37] Tributylphosphine was added to a mixture of resin bound azide and activated amino acid in CH_2Cl_2. The remaining amino acids were coupled as described above.

Initially, compound **4** was synthesized on a 100 μmol scale. At scale-up to 300 μmol extensive epimerization was observed in the cyclization step using DMSO/TFA.[34] The chirality of the LLL-isomers (**4**, **8**, and **12**) and the corresponding epimers (**5**, **9**, and **13**), was elucidated on the basis of comparative HPLC and NMR analysis (chromatograms and ^{1}H NMR spectra are in the Supporting Information). Further assignment of the absolute configuration of the three diastereomeric pairs was established by a combined NMR spectroscopic and computational study.

For the synthesis of analogues **6**, **10**, and **11** (Scheme 2), the appropriate amine was attached to the FMPB AM resin through reductive amination with $NaBH(OAc)_3$ in 1% AcOH/DMF under microwave heating at 60 °C for 20 min.[38] The resulting resin-bound secondary amine was then acylated with Fmoc-Cys(Trt)-OH or Fmoc-Hcy(Trt)-OH overnight using HATU/TMP in CH_2Cl_2/DMF. The first and second steps were monitored by colorimetric tests using the starting resins as references. The presence of CHO groups was evaluated using the *p*-anisaldehyde test,[39] and the existence of secondary amines was examined using the chloranil test.[40,41] Standard couplings described above were used for the second and third amino acid residues. Generally, the oxidative cyclizations were performed under acidic conditions using DMSO/TFA. However, the cyclization of **11** was successfully performed at pH 6 in aqueous AcOH/$(NH_4)_2CO_3$/DMSO.[36]

Methylindole AM resin was used in the synthesis of **7** (Scheme 3) starting with Fmoc deprotection and reaction with Fmoc-Hcy(Trt)-OH overnight. Standard couplings were then carried out for the Fmoc-Tyr(^{t}Bu)-OH and Fmoc-Hcy(Trt)-OH residues. Disulfide cyclization was accomplished using DMSO/TFA.

Configurational Analysis. Small flexible peptides are commonly present in solution as rapidly equilibrating mixtures of low-energy conformations, which cannot be accurately represented by a single structure as conventionally derived by experimentally restrained structure calculations (constrained simulated annealing or restrained molecular dynamics) for proteins.[42] Methods for the deconvolution of time-averaged NMR variables, such as NOEs and scalar couplings, into

Table 1. Stability and Inhibition Activities of Compounds **1**−**13**[d]

No Config	Sequence/Structure	Binding affinity K_i ± SD (nM)[a]		Enzyme K_i ± SD (nM)	
		Chelators	No chelators	IRAP[b]	AP-N[c]
1	Val-Tyr-Ile-His-Pro-Phe	9.3 ± 2.9	1139 ± 1329	62.4 ± 17.5	841 ± 38
2	c[Cys-Tyr-Cys]-His-Pro-Phe	5506 ± 1453	6599 ± 491	16 900 ± 3000	57 000 ± 4900
3	c[Hcy-Tyr-Hcy]-His-Pro-Phe	196 ± 17	1488 ± 89	303 ± 159	5974 ± 1450
4 **LLL**	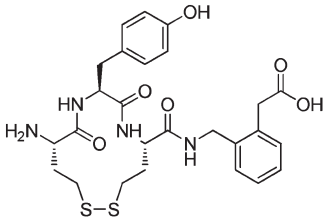	25.3 ± 21.6	1501 ± 1167	22.5 ± 6.0	50 000 ± 36 000
5 **LLD**	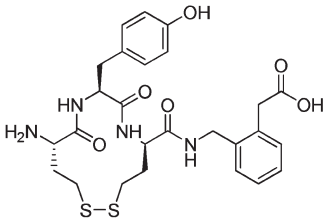	1191 ± 117	10 200 ± 7000	282 ± 113	3588 ± 2293
6 **LLL**	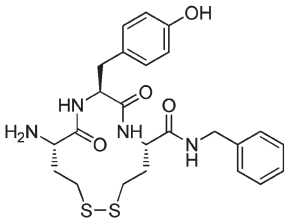	54.8 ± 8.9	13 800 ± 11 500	95.7 ± 26.6	11 100 ± 1900
7 **LLL**	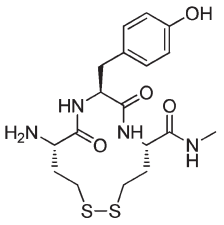			1752 ± 1257	16 800 ± 4800
8 **LLL**	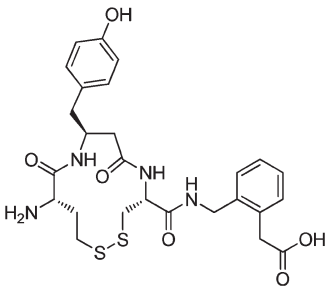	35.1 ± 19.3	1265 ± 6	3.3 ± 0.8	7245 ± 3897
9 **LLD**	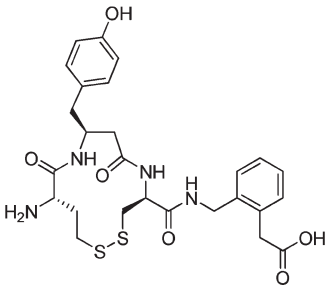	23 100 ± 1000	26 100 ± 700	242 ± 72	10 800 ± 2700

Table 1. Continued

No Config	Sequence/Structure	Binding affinity $K_i \pm$ SD (nM)[a]		Enzyme $K_i \pm$ SD (nM)	
		Chelators	No chelators	IRAP[b]	AP-N[c]
10 **LLL**	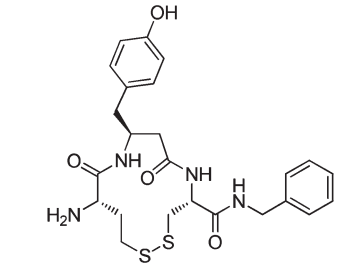	22.5 ± 22.2	3458 ± 191	18.5 ± 4.8	48 900 ± 3700
11 **LLL**	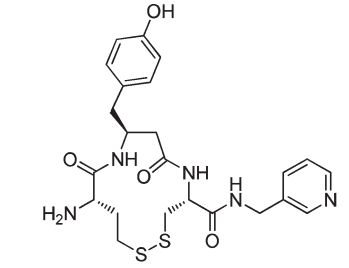	633 ± 93	5416 ± 1666	93.7 ± 9.9	9217 ± 407
12 **LLL**	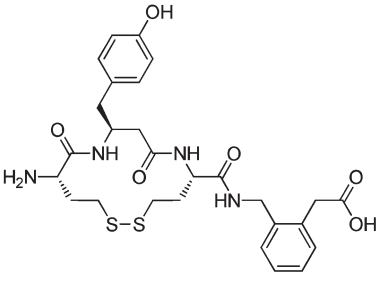	10.0 ± 5.6	357 ± 9	5.2 ± 0.8	5436 ± 2621
13 **LLD**	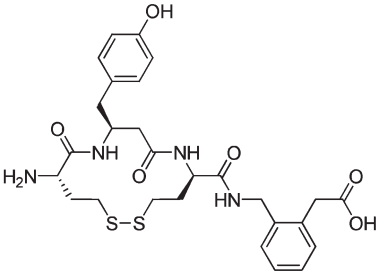	3409 ± 810	13 879 ± 7000	230 ± 53	11 900 ± 5300

[a] [^{3}H]AL-11 competition binding in CHO-K1 cell membranes.[63] [b] Evaluated in an enzyme assay comprising recombinant human IRAP, transiently transfected in HEK293 cells. [c] Evaluated in an enzyme assay comprising recombinant human AP-N, transiently transfected in HEK293 cells. [d] SD, standard deviation.

structural families representing the solution ensemble and fulfilling all structural restraints are available but still seldom utilized.[43−49] In principle, all such techniques generate theoretical ensembles for compounds of known constitution and deconvolute the thermally averaged NMR data to distinct families of conformations. When these conformations are weighted with their probabilities corresponding to their molar fractions, the ensemble fits all experimentally observed distances and dihedrals optimally. For structure elucidation of the diastereomeric pairs **4** and **5**, **8** and **9**, and **12** and **13**, a combined computational and spectroscopic approach was applied, which takes conformational averaging into consideration by ensemble analysis.

Following the reaction route shown in Scheme 1, the synthesis of **4**, **8**, and **12** generated three sets of closely related product pairs giving highly similar NMR spectra and showing comparable chemical properties. Whereas one of the products in each set has the chirality of the starting materials, i.e., L-Hcy[1], L-Tyr[2]/L-β^3hTyr[2], and L-Cys[3]/L-Hcy[3], here denoted LLL (reflecting the configurations of the amino acids in positions 1, 2, and 3), stereomutation of one chiral center of the other isolated compound appears most plausible. Notably, more extensive isomerization would be expected to yield several diastereomeric entities, which was not observed. As described above, a comparison of HPLC retention times and NMR data (Supporting Information Figures S1−S3) of the compounds of unknown chirality with those derived from epimerization-free synthesis (**4**, **6**, **7**, and **10**) indicated an LLL-configuration for compounds **4**, **8**, and **12**, whereas epimerization was predicted for **5**, **9**, and **13**. Assignment of the absolute configuration of the three diastereomeric pairs, confirming the above-described simplified preliminary analysis, was established by a thorough

Scheme 1. Synthesis of **4**, **5**, **8**, **9**, **12**, and **13** Using 2-Chlorotrityl Chloride Resin[a]

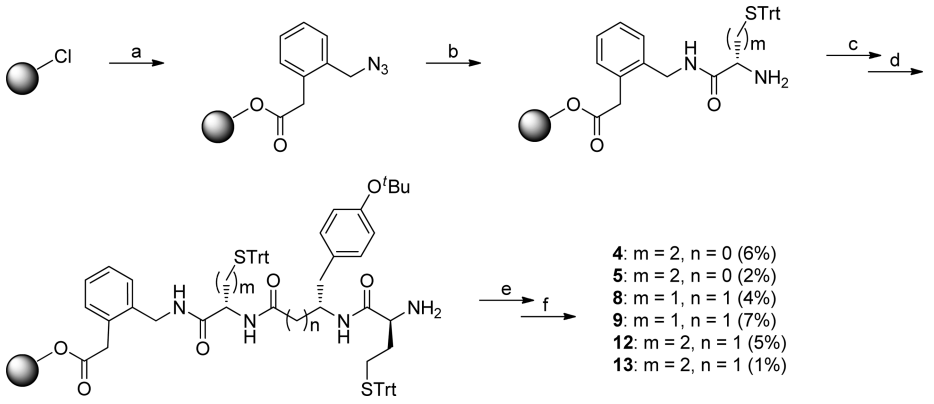

[a] Reagents and conditions: (a) (i) 2-(azidomethyl)phenylacetic acid, DIEA, CH_2Cl_2, room temp, 4 h, (ii) MeOH, 15 min; (b) (i) Fmoc-Cys(Trt)-OH or Fmoc-Hcy(Trt)-OH, DIC, HOBt, CH_2Cl_2, (ii) PBu_3, room temp, on, (iii) 20% piperidine/DMF; (c) (i) Fmoc-Tyr(^{t}Bu)-OH or Fmoc-β^3hTyr(^{t}Bu)-OH, HATU, DIEA, DMF, room temp, 2 h, (ii) 20% piperidine/DMF; (d) (i) Fmoc-Hcy(Trt)-OH, HATU, TMP, CH_2Cl_2/DMF, room temp, 2 h, (ii) 20% piperidine/DMF; (e) DTT, TFA/TES/H_2O (88:5:7), room temp, 2 h; (f) 10% DMSO/TFA, 0 °C to room temp, 6−26 h.

Scheme 2. Synthesis of **6**, **10**, and **11** Using FMPB AM Resin[a]

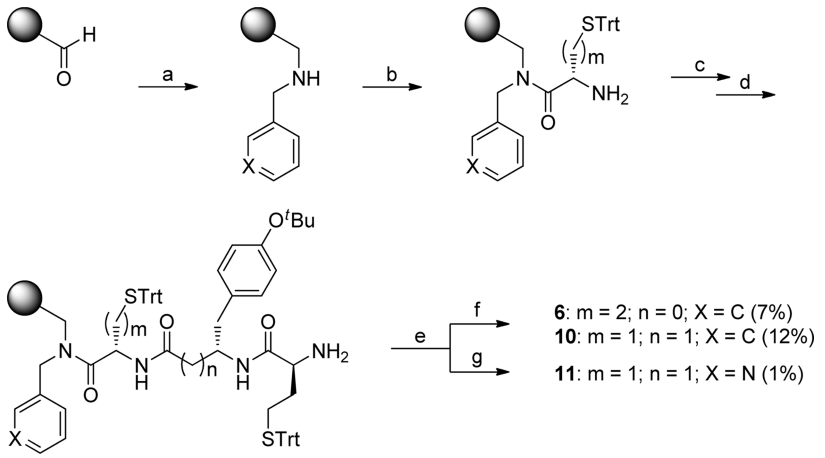

[a] Reagents and conditions: (a) benzylamine or pyridin-3-ylmethanamine (3-picolylamine) (10 equiv), $NaBH(OAc)_3$ (10 equiv), AcOH/DMF (1:99), microwave, 60 °C, 20 min; (b) (i) Fmoc-Cys(Trt)-OH or Fmoc-Hcy(Trt)-OH, HATU, TMP, CH_2Cl_2/DMF, room temp, on, (ii) 20% piperidine/DMF; (c) (i) Fmoc-Tyr(^{t}Bu)-OH or Fmoc-β^3hTyr(^{t}Bu)-OH, HATU, DIEA, DMF, room temp, 2 h, (ii) 20% piperidine/DMF; (d) (i) Fmoc-Hcy(Trt)-OH, HATU, TMP, CH_2Cl_2/DMF, room temp, 2 h, (ii) 20% piperidine/DMF; (e) DTT, TFA/TES/H_2O (88:5:7), room temp, 2 h; (f) 10% DMSO/TFA, 0 °C to room temp, 6−26 h; (g) (i) AcOH (5% aq), $(NH_4)_2CO_3$ (0.5 M aq), pH 6, (ii) DMSO, 0 °C to room temp, on.

NMR spectroscopic study. The applied method is discussed in detail here for the stereoisomeric pair **12** and **13** and summarized for the pair **4** and **5** and the pair **8** and **9** in the Supporting Information.

The feasible conformational populations of the theoretically possible LLL, DLL, LDL, and LLD diastereomers of cyclo[Hcy-β^3hTyr-Hcy]-2-(aminomethyl)phenylacetic acid (AMPA) were predicted by restraint-free systematic Monte Carlo conformational searches (SPMC, 10 000 steps). Throughout these calculations the OPLS-2005 force field and the GB/SA water solvent model were employed, as implemented in the program MacroModel (version 9.0.211), yielding sets of ~250 conformations for each configuration within 10 kcal/mol of the global minimum. The complete set of conformations of c[Hcy-β^3hTyr-Hcy]-AMPA resulting from the unrestrained conformational search revealed an exceptionally high degree of rigidity of the 14-membered macrocycle (Figure 2). The low flexibility of the cyclic peptide results in a very limited number of possible steric arrangements of the central core of its four theoretically obtainable epimers (Figure 3). Significant differences in the CH^{α} hydrogen orientation of the possible stereoisomers allow their differentiation by applying NOE-based distance and scalar coupling-derived dihedral angle measurements.

Configurations were assigned through deconvolution of the experimentally acquired NOEs and $^3J_{HH}$ coupling constants into computationally predicted ensembles of the four theoretically possible diastereomers of **12** and comparison of the quality of the fits between the experimental and the computed data of the various stereoisomers. In order to ensure the best possible coverage of the conformational space,[50] we also performed a second Monte Carlo search using the Amber* force field, yielding a total set of 700−950 distinct conformations for each theoretical stereoisomer (LLL, DLL, LDL, LLD).

Subsequently, for each diastereomer, the set of conformations best fitting the experimental data (NOE and $^3J_{HH}$) was derived using the NAMFIS program,[47] and the probabilities of the conformations were predicted. The root-mean-square deviations (rmsd) of the back-calculated intramolecular distances and J couplings of the probability-weighted averages of the selected conformational ensembles, compared to the observed experimental NMR data, were evaluated for

Scheme 3. Synthesis of **7** Using Methylindole AM Resin[a]

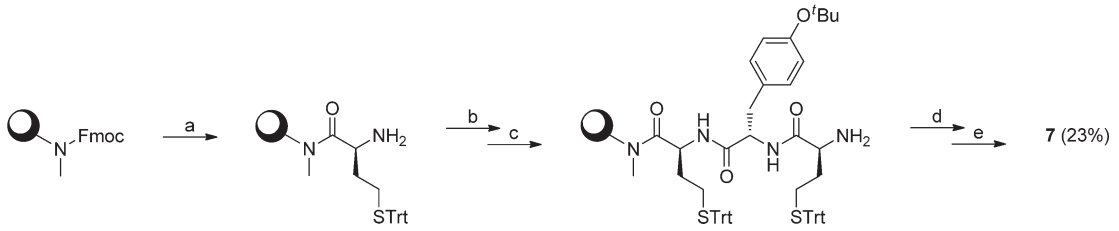

[a] Reagents and conditions: (a) (i) 20% piperidine/DMF, (ii) Fmoc-Hcy(Trt)-OH, HATU, TMP, CH_2Cl_2/DMF, room temp, on, (iii) 20% piperidine/DMF; (b) (i) Fmoc-Tyr(^{t}Bu)-OH, HATU, DIEA, DMF, room temp, 2 h, (ii) 20% piperidine/DMF; (c) (i) Fmoc-Hcy(Trt)-OH, HATU, TMP, CH_2Cl_2/DMF, room temp, 2 h, (ii) 20% piperidine/DMF; (d) DTT, TFA/TES/H_2O (88:5:7), room temp, 2 h; (e) 10% DMSO/TFA, 0 °C to room temp, 23 h.

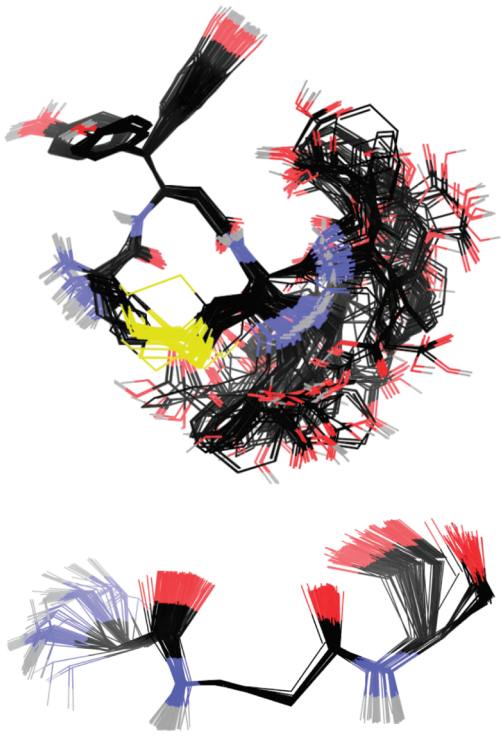

Figure 2. An overlay of the backbones of all (228) conformations of c[Hcy-β^3hTyr-Hcy]-AMPA, within 10 kcal/mol (42 kJ/mol) of the global minimum generated by a restraint-free systematic Monte Carlo conformational search, is shown above, whereas a magnification of the backbone atoms of Hcy-β^3hTyr-Hcy is depicted below. Side chain atoms are omitted for clarity. A remarkable rigidity of the central cyclic core is indicated, as well as well-defined orientations of the CH^{α} and amide NH protons, despite some flexibility in the disulfide region.

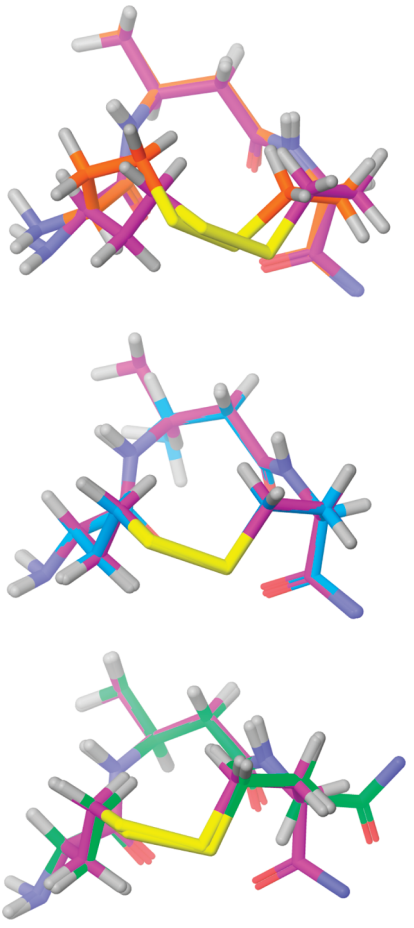

Figure 3. Overlay of the backbones of the native LLL-configuration and the lowest energy conformations of the possible epimers of c[Hcy-β^3hTyr-Hcy]-AMPA (compounds **12** and **13**, as depicted in Table 1). The color coding is as follows: LLL pink, DLL orange, LDL blue, and LLD green. The overlaps indicate a highly similar orientation of the central core of the diastereomers. Discrimination between the isomers is only possible by differentiation of the orientation of Hcy^1-H^{α} for the DLL–LLL pair, β^3hTyr^2-H^{β} for the LDL–LLL pair, and Hcy^3-H^{α} for the LLD–LLL pair.

identification of the best fitting configuration. The goodness of fit was expressed as the sum of the square differences (SSD) between the measured and modeled variables (a lower SSD reflects a better fit), as previously described by Snyder et al.[42] Sets of 37 and 18 critical NOEs were used, together with 16 and 8 $^3J_{HH}$ values, for compounds **12** and **13**, respectively (Supporting Information pp S13−S14). The different numbers of experimental parameters included in the calculations reflect the larger degree of signal overlaps for compound **13**, allowing the determination of a larger number of precise distance and dihedral constraints for **12** compared to **13**. To minimize the uncertainty of the structure determination of the main ring, NOEs and $^3J_{HH}$ values originating from the comparably more flexible AMPA residue and the side chain of β^3hTyr^2 (Figure 2) were excluded from this analysis. The best fit between the NMR data and the ensemble selected by NAMFIS was obtained for the LLL-configuration of compound **12** (SSD values as follows: LLL = 1.28; LLD = 7.24; LDL = 1.84; DLL = 3.33) and the LLD-configuration of **13** (LLL = 20.7; LLD = 14.0; LDL = 26.6; DLL = 42.4),[86] which fulfilled the experimental restraints without any significant deviation (Supporting Information pp S13−S14). Further investigations using the NAMFIS program allowed the determination of the configuration of compounds **4** and **5** and compounds **8** and **9** (**4**, LLL; **5**, LLD; **8**, LLL; **9**, LLD). This finding was further confirmed by small scale, epimerization-free preparation of analogue **4**.

We emphasize that NAMFIS analysis was originally developed for the prediction of the available conformational space of compounds of known configuration. Its application to the elucidation of the configuration of Ang IV analogues is novel, and was possible because of the unusual rigidity of the central tripeptidic core of the investigated peptides, and cannot be generalized. The applied method, similar to other available NMR techniques, enables only the determination of the absolute configuration of a stereocenter in case the chirality of at least one additional chiral center in the proximity is known. Previously published NMR methods for the determination of the relative configuration of organic molecules use the combination of H−H scalar coupling constants and local NOEs; however, they require at least one additional parameter such as two- or three-bond H−C scalar couplings[51,52] and/or residual dipolar couplings.[53] Methods for the determination of configurations based on residual dipolar couplings only are also available.[54−56] A common feature of these techniques is the requirement of comparably large amounts (preferably tenths of milligram) of investigated substance, since they necessitate the observation of heteronuclear coupling constants. To us only 0.4−4 mg samples of the discussed compounds were available for NMR analysis and such methods were therefore unsuitable.

The fact that extensive epimerization was observed only for the compounds containing AMPA in the C-terminal suggests that the carboxyl group might be involved in interactions favoring epimerization in position 3.

Biochemical Evaluation. The ability of **1**−**13** to inhibit the catalytic activity of recombinant human IRAP and aminopeptidase N (AP-N) transiently transfected in HEK293 cells was examined and compared. Furthermore, the stability of **1**−**6** and **8**−**13** toward degradation by metallopeptidases in membrane homogenates was investigated. To this end, membranes of endogenous IRAP-containing CHO-K1 cells were preincubated with different concentrations of compounds in either the absence or presence of chelators and then further incubated with a radioligand in the presence of chelators. Binding affinities in the continuous presence of chelators refer to the IRAP apo-enzyme.[57,58] When preincubation proceeds in the absence of chelators, the competition curve will shift to the right if the compound is rapidly degraded by IRAP and/or other metallopeptidases. The binding affinities and IRAP activity inhibition data of the compounds are presented in Table 1.

It is well accepted that wide structural variations can be performed in the C-terminal tripeptide of Ang IV with retained biological activity.[59−62] We previously reported that replacement of His^4-Pro^5-Phe^6 in Ang IV with an AMPA moiety rendered a ligand with an equipotent binding affinity and IRAP inhibitory activity to Ang IV.[30] Conversely, small variations in the N-terminal region had considerable effects on the activity. We imposed steric constraints at the N-terminals via disulfide cyclizations in order to identify bioactive conformations of Ang IV.[31] An 11-membered ring system was created by the cyclization of Cys^1 with Cys^3 in an Ang IV analogue where Val^1 and Ile^3 had been displaced. This maneuver was found to be deleterious to the activity (**2**, K_i = 16 900 nM). Incorporation of a simpler one-residue backbone mimetic, i.e., replacement of the Tyr^2 residue in Ang IV by a 4-hydroxydiphenylmethane scaffold, was also nonproductive.[29] However, formation of a 13-membered ring system via an Hcy^1/Hcy^3 cyclization afforded an IRAP inhibitor (**3**, K_i = 303 nM), albeit 5 times less potent than Ang IV itself (**1**, K_i = 62.4 nM). Thus, a bioactive conformation can be adopted after cyclization, but a ring system of greater conformational flexibility than Cys^1/Cys^3 seems to be required for appropriate spatial orientation of the side chains in the N-terminal of Ang IV.[31]

Figure 4. Overlaid backbones of the low energy conformations of the bioactive **4** (orange), **8** (purple), and **12** (green) indicate comparable orientation of the functionalities that may be involved in the molecular recognition process responsible for their IRAP inhibitory activity. Enlargement of the carbon ring by one atom does not significantly alter the location of the amino acid side chains or that of the attached AMPA residue.

As can be seen in Table 1, compound **4**, comprising a 13-membered disulfide ring system and a C-terminal 2-(aminomethyl)phenylacetic acid group, is a more efficient IRAP inhibitor (K_i = 22.5 nM) than Ang IV and exhibits higher selectivity over AP-N. The large difference between the K_i values obtained from the binding assays, with and without chelators, suggests that **4** is rapidly degraded in the CHO-K1 cell membranes just as Ang IV. The chelators serve to block the proteolytic activity of IRAP, AP-N, and other metallopeptidases.[58,64] Epimer **5** is 10 times weaker as an inhibitor of IRAP than **4** and exhibits lower selectivity over AP-N. As shown in previous studies, a C-terminal carboxyl group is preferred (cf. **4** and **6**).[30] Also, removal of the aromatic moiety in the C-terminal part is deleterious to the activity (cf. **4** and **7**). Retaining the ring size but replacing Hcy^3 by Cys and Tyr^2 by a β-amino acid residue renders an alternative 13-membered disulfide ring system. This modification led to a very potent IRAP inhibitor, compound **8** (K_i = 3.3 nM), which was 10 times more potent than **4** and 20 times more potent than Ang IV itself. The epimer **9** is considerably less active. As was the case with **4**, the removal of the carboxyl group from **8** results in a less active inhibitor (**10**, K_i = 18.5 nM), but this macrocyclic disulfide is still 3 times more potent than the parent compound Ang IV. Contrary to the carboxyl analogue **8**, compound **10** is essentially devoid of all AP-N inhibitory activity. There are previous reports of linear Ang IV analogues containing nitrogen heteroaromatics (e.g., 2-quinolyl and 4-pyridyl) in the C-terminal end, with good affinity to the Ang IV binding sites (AT_4 receptor/IRAP).[59,60] However, as reported here, the replacement of the phenyl moiety in **10** by 3-pyridyl in the C-terminal, giving **11**, resulted in a less effective inhibitor of IRAP which exhibited low selectivity. A comparison of **4** or **8** with inhibitor **12** reveals the possibility of ring enlargement without losing IRAP inhibiting capacity (Figure 4). Epimer **13** possess lower activity

also in this case. The NMR-based configuration analysis indicated that **5**, **9**, and **13** were epimerized at the amino acid residue in position 3, revealing the high importance of the configuration in this position for IRAP activity because the LLD epimers are considerably less active than their corresponding LLL epimers.

All of the IRAP inhibitors **2**−**4**, **8**, **10**, and **12** exhibited low metabolic stability. Thus, cyclization did not make the N-terminal peptide bond resistant to proteolysis by IRAP and/or other metallopeptidases present in the CHO-K1 cell membranes. This observation is not unexpected, since vasopressin and oxytocin, both substrates for IRAP, contain an N-terminal disulfide-bridged cyclic hexapeptide and both peptides are subjected to N-terminal sequential degradation by IRAP.[65−67] The incorporation of a β-amino acid residue to replace Tyr^2 (i.e., β^3hTyr) did not improved the proteolytic stability. However, as shown in the example of the metabolically stable β^2hVal^1-Ang IV by Lukaszuk et al.,[27] modification of the N-terminal amino acid residue significantly improves proteolytic stability. As an IRAP inhibitor, β^2hVal^1-Ang IV was slightly less efficient (K_i = 100 nM). The hexapeptide Val-β^3hTyr-Ile-His-Pro-Phe was also found to be less potent than Ang IV (K_i = 173 nM).[27] The replacement of Tyr^2 in this Ang IV analogue[27] with a β-homoamino acid residue and most other modifications centered around Tyr^2 provide less potent peptides/pseudopeptides.[29,30] It is therefore notable that the cyclized disulfides **8**, **10**, and **12**, all comprising β^3hTyr^2, are among the most potent IRAP inhibitors reported to date. As previously deduced from theoretical conformational analysis and ^{1}H NMR spectroscopy, oxidative cyclization of Cys^3-Tyr^4-Cys^5-Ang II creates an 11-membered ring system prone to adopt γ-turns.[68] In contrast, Hcy^3-Tyr^4-Hcy^5-Ang II forms a 13-membered ring system comprising a disulfide unit with a large number of low-energy conformations including one γ-turn and one β-turn conformation, but no preferred well-defined conformation was identified.[68] Since the corresponding Cys^1-Tyr^2-Cys^3-Ang IV **2** is essentially inactive as IRAP inhibitor,[31] it thus appears that a γ-turn is not adopted upon interaction with IRAP. Further data acquisition is needed in order to elucidate the conformation optimal for IRAP inhibition. Coordination to the catalytic zinc ion in IRAP by elements in the N-terminal is expected to have a pronounced effect on the conformation and the binding mode of conformationally flexible inhibitors.[67,69−73]

Conclusion

We have demonstrated that oxidative cyclization of the Ang IV analogue Hcy-Tyr-Hcy-His-Pro-Phe provides an IRAP inhibitor **3** (K_i = 303 nM) 5 times less potent than Ang IV, whereas replacement of the C-terminal tripeptide His-Pro-Phe of **3** by a phenylacetic acid moiety resulted in a 2-fold increase in inhibitory activity (**4**, K_i = 22.5 nM). Moreover, further increased potency was obtained by replacing Tyr^2 in **4** with β^3hTyr and Hcy^3 with Cys, followed by cyclization; compound **12** with a 14-membered ring system exhibits a K_i of 5.2 nM, and compound **8** encompassing a 13-membered ring system exhibits a K_i of 3.3 nM. A pronounced impact of the spatial arrangement of the functional groups at the C-terminal end on IRAP inhibitory activity was revealed by the lower potency of the corresponding LLD epimers **13** and **9** compared to Ang IV. Compounds **8** and **12** are among the most potent IRAP inhibitor reported to date.

Experimental Section

General Information. Microwave heated reactions were performed in a Smith Synthesizer (Biotage AB, Uppsala, Sweden) producing controlled irradiation at 2450 MHz. Analytical RP-HPLC−MS was performed on a Gilson HPLC system with a Finnigan AQA quadrupol mass spectrometer using an Onyx monolithic C18 column (4.6 mm × 50 mm) with gradients of CH_3CN/H_2O (0.05% HCOOH) or MeOH/H_2O (0.05% HCOOH) at a flow rate of 4 mL/min. Both UV (DAD, 214 and 254 nm) and MS (ESI) detection were utilized. Preparative RP-HPLC was performed using a Zorbax SB-C8 column (5 μm, 21.2 mm × 150 mm) with gradients of CH_3CN/H_2O (0.1% TFA) at a flow rate of 5 mL/min and UV detection at 230 nm. The purity of the compounds was determined on a Zorbax SB-C8 (5 μm, 4.6 mm × 50 mm) and an Allure Biphenyl column (5 μm, 4.6 mm × 50 mm) using the same buffer systems at a flow rate of 2 mL/min and with UV detection at 220 nm. Optical rotations were obtained on a Perkin-Elmer 241 polarimeter. Specific rotations ($[\alpha]_D$) are reported in deg/dm, and the concentration (c) is given as g/100 mL in the specified solvent. NMR spectra were recorded on a Varian Mercury Plus spectrometer (^{1}H at 400 MHz and ^{13}C at 101 MHz) at ambient temperature. Chemical shifts (δ) are reported in ppm referenced indirectly to TMS via the ^{2}H lock signal. Assignment was made by gCOSY, gHSQC, and gHMBC experiments. Exact molecular masses were determined on a Micromass Q-Tof2 mass spectrometer equipped with an electrospray ion source at the Department of Pharmaceutical Biosciences, Uppsala University, Sweden. Elemental analysis was performed at Mikrokemi AB, Uppsala, Sweden. The manual solid-phase synthesis was performed in disposable syringes fitted with porous polyethylene filters, and a Stuart SB2 tube rotator was used for agitation. The resins were purchased from Novabiochem. Dichloromethane used in the reactions was distilled over calcium hydride. Other chemicals were purchased and used without further purification. Final product yields were determined on the basis of the initial loading of the resin. The final compounds were more than 97% pure as assessed from analytical RP-HPLC analysis. The synthesis of 2-(azidomethyl)phenylacetic acid[29] and analogues **1**−**3**[31] has been described previously.

General Procedure A: Attachment of 2-(Azidomethyl)phenylacetic Acid to 2-Chlorotrityl Chloride Resin. 2-(Azidomethyl)-phenylacetic acid[29] (1.0 equiv) was reacted with 2-chlorotrityl chloride resin (1.5 equiv) in CH_2Cl_2 in the presence of DIEA (4.0 equiv). After 5−7 h, MeOH was added and the mixture was stirred for at least 15 min before the resin was transferred to a 5 mL disposable syringe fitted with a porous polyethylene filter, washed with several portions of, in turn, CH_2Cl_2, DMF, MeOH, and CH_2Cl_2, and dried in vacuo.

General Procedure B: Reductive Amination of FMPB AM Resin. FMPB AM resin, $NaBH(OAc)_3$ (10 equiv) and DMF were added to a 10−20 mL Biotage microwave vial containing a stirring bar. After being sealed, the vial was flushed with nitrogen gas and the appropriate amine (10 equiv) and AcOH (cat.) were added. The reaction mixture was heated to 60 °C by microwave irradiation for 20 min, cooled to room temperature, and transferred to a 5 mL disposable syringe fitted with a porous polyethylene filter. The resin was washed with several portions of, in turn, DMF, MeOH, and CH_2Cl_2 and dried in vacuo. Two colorimetric tests were employed to examine the reaction: the *p*-anisaldehyde test to detect the presence of CHO groups[39] and the chloranil test[40,41] to detect the presence of secondary amines. The FMPB AM resin was used as a reference.

General Procedure C: Fmoc Deprotection and Coupling to Methylindole AM Resin. Methylindole AM resin was weighed into a 5 mL disposable syringe fitted with a porous polyethylene filter and swollen in CH_2Cl_2 for approximately 1 h. The solvent was replaced by DMF, and the Fmoc group was removed by treatment with 20% piperidine in DMF (2 × 3 mL) followed by repeated rinsing with DMF. The liberated secondary amine was coupled with the appropriate amino acid (2.0 equiv) overnight in

CH_2Cl_2/DMF 4:1 using HATU (2.0 equiv) in the presence of TMP (4.0 equiv). After the resin was washed with DMF, the Fmoc group was removed as described above. Subsequent to DMF, several portions of MeOH and CH_2Cl_2 were used to rinse the resin which was then dried in vacuo or immediately used in the following step. The chloranil test was used to monitor the reaction.[40,41] The Fmoc deprotected methylindole AM resin was used as a reference.

General Procedure D: Coupling to 2-(Azidomethyl)phenylacetyl-2-chlorotrityl Resin. A round-bottomed flask was charged with the appropriate amino acid (3.0 equiv), HOBt (3.0 equiv), and DIC (3.0 equiv) in dry CH_2Cl_2. After preactivation under nitrogen for 10 min, 2-(azidomethyl)phenylacetyl-2-chlorotrityl resin (1.0 equiv) was added, followed by PBu_3 (2.0 equiv) 10 min later. The reaction mixture was stirred under nitrogen for 6 h and then transferred to a 5 mL disposable syringe fitted with a porous polyethylene filter. The resin was washed with several portions of, in turn, CH_2Cl_2, DMF, MeOH, and CH_2Cl_2 and dried in vacuo.

General Procedure E: Coupling and Deprotection of Cysteine and Homocysteine Residues. Unless otherwise stated, a solution of Fmoc-Cys(Trt)-OH (1.5 equiv), HATU (1.5 equiv), and TMP (3.0 equiv) in CH_2Cl_2/DMF or Fmoc-Hcy(Trt)-OH (1.1 equiv), HATU (1.1 equiv), and either TMP (2.2 equiv) or DIEA (2.2 equiv) in CH_2Cl_2/DMF or DMF was added to the resin, and the reaction mixture was agitated by rotation for 2 h (primary amines) or overnight (secondary amines). To remove the Fmoc group, the resin was treated with 20% piperidine in DMF (2 × 3 mL) and then washed with several portions of DMF. After completion of the coupling cycle the resin was also washed with several portions of, in turn, CH_2Cl_2, MeOH, and CH_2Cl_2 and dried in vacuo. In some cases DIEA was used insted of TMP in the last coupling of Fmoc-Hcy(Trt)-OH.

General Procedure F: Coupling and Deprotection of Tyrosine and β-Homotyrosine Residues. Unless otherwise stated, the amino acids were coupled according to general method E above, using Fmoc-Tyr(^{t}Bu)-OH (3.0 equiv), HATU (3.0 equiv), DIEA (6.0 equiv) or Fmoc-β^3hTyr(^{t}Bu)-OH (1.1 equiv), HATU (1.1 equiv), and DIEA (2.2 equiv) in DMF.

General Procedure G: Resin Cleavage, Side Chain Deprotection, and Purification. The resin was transferred from the disposable syringe to a 50 mL Falcon tube containing a stirring bar. The resin was treated with a mixture of 95% TFA (2.1 mL), TES (150 μL), and DTT (0.01 g, 64.8 μmol) under gentle stirring for 2 h. CH_3CN was added to dissolve any precipitate formed before the resin was filtered off and further washed with CH_3CN. The filtrate was evaporated, and the residue was dissolved in CH_3CN. Water was added, resulting in a precipitate which was filtered off. The filtrate was freeze-dried, and the resulting product was dissolved in CH_3CN/H_2O (0.1% TFA), filtered through a 0.45 μm nylon membrane, and purified with RP-HPLC. Selected fractions were analyzed by RP-HPLC and RP-HPLC−MS, and those containing pure product were pooled and lyophilized to give the pure product as the TFA salt.

General Procedure H: Disulfide Bridge Formation and Purification.[34] S−S oxidation was achieved by dissolving the linear peptide in TFA at 3 mg/mL, adding DMSO at 0 °C to give a final concentration of 10−15% (v/v) and then maintaining the reaction mixture at room temperature until HPLC analysis showed oxidation to be complete. After concentration in a stream of nitrogen and coevaporation with toluene, the residue was diluted with CH_3CN/H_2O (0.1% TFA), filtered through a 0.45 μm nylon membrane, and purified with RP-HPLC. Selected fractions were analyzed by RP-HPLC and RP-HPLC−MS, and those containing pure product were pooled and lyophilized to give the product as the TFA salt.

General Procedure I: Disulfide Bridge Formation and Purification.[36] The linear peptide was dissolved in 5% AcOH at 1.5 mM. The pH was adjusted to 6 using $(NH_4)_2CO_3$ (0.5 M, aq). DMSO was added to the solution at 0 °C to give a final concentration of 10−15% (v/v). The reaction mixture was stirred at 0 °C for 10 min and then at room temperature until HPLC analysis showed oxidation to be complete. The reaction mixture was diluted 2-fold with CH_3CN/H_2O (0.1% TFA), filtered through a 0.45 μm nylon membrane, and purified with RP-HPLC. Selected fractions were analyzed by RP-HPLC and RP-HPLC−MS, and those containing pure product were pooled and lyophilized to give the product as the TFA salt.

c[Hcy-Tyr-Hcy]AMPA (4) and c[Hcy-Tyr-D-Hcy]AMPA (5). Solid-phase attachment was performed according to general procedure A using 2-(azidomethyl)phenylacetic acid (122 mg, 636 μmol), 2-chlorotrityl chloride resin (683 mg, 962 μmol), DIEA (443 μL, 2.54 mmol), and CH_2Cl_2 (6.0 mL). MeOH (1.0 mL) was added after 7 h, and stirring was continued for 40 min. Yield: 738 mg. Part of the resin (352 mg, 303 μmol) was then reacted with Fmoc-Hcy(Trt)-OH (268 mg, 447 μmol), as described in procedure D, using HOBt (63.4 mg, 469 μmol), DIC (67 μL, 430 μmol), 85% PBu_3 (75 μL, 430 μmol), and CH_2Cl_2 (10 mL). The subsequent coupling of Fmoc-Tyr(^{t}Bu)-OH (401 mg, 873 μmol) was performed with HATU (338 mg, 889 μmol) and DIEA (300 μL, 1.72 mmol) in DMF (3 mL) following general method F. General procedure E was applied for the coupling of the N-terminal Fmoc-Hcy(Trt)-OH (250 mg, 418 μmol) residue using HATU (165 mg, 433 μmol) and TMP (114 μL, 861 μmol) in CH_2Cl_2 (2.4 mL) and DMF (1.0 mL). Deprotection and cleavage from the resin following general procedure G yielded the linear sequence (46.3 mg, 68.4 μmol), which was subjected to disulfide bridge formation according to general method H using TFA (15.4 mL) and DMSO (2.44 mL). The last step gave a mixture of two epimers, **4** and **5**, which could be separated by RP-HPLC.

c[Hcy-Tyr-Hcy]AMPA (4). The product was isolated as the TFA salt (11.5 mg, 6%). $[\alpha]^{21}_D$ −38.5° (*c* 0.21, 0.1% TFA in CD_3OD/D_2O 9:1). ^{1}H NMR (400 MHz, CD_3OD) δ 7.28−7.22 (m, 4H, ArH), 7.08 (m, 2H, Tyr-H2, Tyr-H6), 6.65 (m, 2H, Tyr-H3, Tyr-H5), 4.75 (m, 1H, Tyr-H$^\alpha$), 4.49 (dd, J = 10.9, 4.0 Hz, 1H, Hcy^3-H$^\alpha$), 4.40 (d, J = 15.2 Hz, 1H, NCH_{2a}), 4.35 (d, J = 15.2 Hz, 1H, NCH_{2b}), 3.94 (dd, J = 6.0, 3.4 Hz, 1H, Hcy^1-H$^\alpha$), 3.72 (app s, 2H, CH_2CO), 3.09 (dd, J = 13.9, 7.6 Hz, 1H, Tyr-H$^\beta$), 2.98−2.79 (m, 3H, Hcy^3-H$^\gamma$, Hcy^3-H$^{\gamma'}$, Tyr-H$^{\beta'}$), 2.77−2.64 (m, 2H, Hcy^1-H$^\gamma$, Hcy^1-H$^{\gamma'}$), 2.29−2.10 (m, 3H, Hcy^1-H$^\beta$, Hcy^1-H$^{\beta'}$, Hcy^3-H$^\beta$), 1.99 (m, 1H, Hcy^3-H$^{\beta'}$). ^{13}C NMR (101 MHz, CD_3OD) δ 175.4, 173.2, 172.3, 169.0, 157.4, 137.9, 134.3, 131.9, 131.4, 129.5, 128.8, 128.7, 128.6, 116.4, 56.1, 53.4, 52.6, 41.9, 39.1, 36.6, 35.0, 31.5, 31.3, 31.2. HPLC purity: C8 column 99.5%, biphenyl column 99.8%. HRMS (M + H$^+$): 561.1849, $C_{26}H_{33}N_4O_6S_2$ requires 561.1842. Anal. Calcd for $C_{26}H_{32}N_4O_6S_2 \cdot CF_3COOH \cdot 0.8H_2O$: C, 48.80; H, 5.06; N, 8.13; S, 9.31. Found: C, 48.70; H, 5.10; N, 7.90; S, 9.40.

c[Hcy-Tyr-Hcy]NHMe (7). Solid-phase attachment was done according to general procedure C using methylindole AM resin (300 mg, 189 μmol), Fmoc-Hcy(Trt)-OH (231 mg, 385 μmol), HATU (165 mg, 433 μmol), and TMP (100 μL, 756 μmol) in CH_2Cl_2 (3.2 mL) and DMF (0.8 mL). Subsequently, the resin was reacted with Fmoc-Tyr(^{t}Bu)-OH (274 mg, 596 μmol) as described in procedure F using HATU (221 mg, 560 μmol), DIEA (1.14 mmol, 199 μL), DMF (3 mL). Procedure E was applied for the coupling of the N-terminal Fmoc-Hcy(Trt)-OH (153 mg, 255 μmol) residue using HATU (149 mg, 393 μmol), TMP (100 μL, 760 μmol), CH_2Cl_2 (2.4 mL), and DMF (2.0 mL). Deprotection and cleavage from the resin following the general procedure G yielded the linear sequence (48.7 mg, 89.8 μmol), which was subjected to disulfide bridge formation according to general method H using TFA (16.2 mL) and DMSO (1.62 mL). The product was isolated as the TFA salt (23.1 mg, 23%).

c[Hcy-β^{3}hTyr-Cys]NH(3-picolyl) (11). Solid-phase attachment was done according to general procedure B using FMPB AM resin (265 mg, 259 μmol), pyridin-3-ylmethanamine (260 μL, 2.55 mmol), $NaBH(OAc)_3$ (548 mg, 2.58 mmol), AcOH (0.05 mL), DMF (4.95 mL). The resin was then reacted with Fmoc-Cys(Trt)-OH (457 mg, 780 μmol) as described in procedure E using HATU (297 mg, 780 μmol), TMP (205 μL, 1.55 mmol),

CH_2Cl_2 (2.4 mL), and DMF (0.6 mL). The subsequent coupling of Fmoc-β^3hTyr(^{t}Bu)-OH (137 mg, 288 μmol) was performed with HATU (109 mg, 285 μmol, 1.1 equiv) and DIEA (99 μL, 569 μmol) in DMF (3.0 mL) following general method F. Procedure E was applied for the coupling of the N-terminal Fmoc-Hcy(Trt)-OH (179 mg, 298 μmol) residue using HATU (109 mg, 286 μmol) and TMP (75 μL, 570 μmol) in CH_2Cl_2 (2.4 mL) and DMF (0.6 mL). Deprotection and cleavage from the resin following the general procedure G yielded the linear sequence (2.6 mg, 3.5 μmol), which was subjected to disulfide bridge formation according to general method I using 5% AcOH (2.8 mL), 0.5 M $(NH_4)_2CO_3$ (2.2 mL), and DMSO (0.6 mL). The product was isolated as the TFA salt (1.6 mg, 1%).

NMR Spectroscopy Experiments and Computational Studies. NMR studies were carried out using Varian Unity INOVA spectrometers (^{1}H at 900, 800, and 600 MHz) at 25 °C. Assignment was made using NOESY, TOCSY, gCOSY, gHSQC, and gHMBC experiments. Samples were dissolved in DMSO-d_6 (Aldrich) for complete assignment including amide protons. On the basis of previous experience, we assumed that using DMSO instead of D_2O would cause a slight redistribution of conformation populations rather than result in the formation of completely different orientations.[50] Hence, the conformations identified in DMSO-d_6 are relevant in biological context. NOE build-up studies were performed using the conventional "three-$\pi/2$" NOESY pulse sequence[74,75] without solvent suppression, with mixing time of 40, 80, 120, 160, 200, 300, 400, or 500 ms. The relaxation delay was set to 2.5 s; 16 scans were accumulated, and 4096 and 512 points were used in the direct and indirect dimensions, respectively. Interproton distances were calculated using the initial rate approximation and the internal calibration distance between germinal methylene protons (1.78 Å; Cys-H$^\beta$, Hcy-H$^\beta$, and β^3hTyr-H$^\gamma$), as calculated by comparison of the relative build-up rates ($r_{ij} = r_{\mathrm{ref}}(\sigma_{\mathrm{ref}}/\sigma_{ij})^{(1/6)}$, where r_{ij} denotes the distance between protons i and j and σ_{ij} is the normalized intensity of their NOE). At least five mixing times yielding a linear ($r^2 > 0.95$) initial NOE rate were used to estimate the σ_{ij} build-up rates. Peak intensities were calculated using normalization of both cross-peaks with both diagonal peaks ($[(\mathrm{xpeak}_1 \times \mathrm{xpeak}_2)^2/(\mathrm{diagpeak}_1 \times \mathrm{diagpeak}_2)^2]^{0.5}$). Vicinal coupling constants were derived from ^{1}H NMR or E-COSY spectra[76] using 4096 × 1024 data points followed by zero-filling up to 8192 × 8192 points.

Theoretical Conformational Analysis. Conformational energy calculations were performed using the systematic search method SPMC. To ensure that the entire potential energy surface is covered, separate calculations using the OPLS-2005 and the Amber* all atom force fields were employed as implemented in the program MacroModel 9.02.[77] The general Born solvent accessible (GB/SA) surface area method developed by Still was used in all calculations.[78] The number of torsion angles allowed to vary during each Monte Carlo step ranged from 1 to $n - 1$ where n equals the total number of rotatable bonds. Amide bonds were fixed in the trans configuration. For each force field, 10 000 Monte Carlo steps were performed in separate calculations, followed by a maximum of 5000 PR conjugate gradient minimization steps, and a cutoff of 1.0 Å was applied; conformations within 42 kJ/mol of the global minimum were retained. Still et al. have suggested that locating the global minimum at least 7−12 times constitutes a thorough search of a molecule's potential energy surface.[77] The global minimum was found at least 20 times in all calculations. The OPLS-2005 force field, used in the theoretical analysis, had no low quality parameters and, apart from three medium torsions used, only high quality stretching, bending, and torsional parameters. The Amber force field had no low quality parameters but had 6, 18, and 55 medium quality stretch, bend, and torsion parameters in addition to the 332 high quality ones.

NAMFIS Analysis. Unrestrained conformational searches in OPLS-2005 and Amber force fields yielded a total of 700−950 optimized theoretical conformations for each analyzed structure. The list of NOEs and J couplings observed for compounds **4**, **5**, **8**, **9**, **12**, and **13** are presented together with $^3J_{\mathrm{HH}}$ values in the Supporting Information. In the NAMFIS analysis only NOEs between hydrogens directly bound to the heavy atoms of the macrocyclic ring were applied to eliminate possible errors introduced by an incomplete set of conformations of the side chains. The NAMFIS program deconvolutes the averaged NMR spectrum of a compound into weighted contributions from theoretical conformers[47] by performing a least-squares fit of NOE-derived distances, and $^3J_{\mathrm{HH}}$ values to the corresponding data were back-calculated for each theoretical conformer. In other words it varies the mole fraction of each optimized conformer until the best possible fit to the available set of conformations is obtained. Goodness of fit is expressed as the "sum of the square differences" (SSD) and the root-mean-square deviation (rmsd) values between the experimental and computed data.

The $^3J_{\mathrm{NH\text{-}H}\alpha}$ couplings used in the NAMFIS analysis were calculated for each computed conformation using the extended Karplus equation developed for peptides.[79,80] Corresponding $^3J_{\mathrm{HH}}$ values for the vicinal protons attached to carbons only were derived for the theoretically predicted conformers by the equation presented by Haasnoot, De Leeuw, and Altona.[81]

Biochemical Evaluation. L-Leucine-*p*-nitroanilide (L-Leu-pNA) was obtained from Sigma-Aldrich. [^{3}H]AL-11 was obtained from G. Tóth, Biological Research Center (Szeged, Hungary).[63] All other reagents were of the highest grade commercially available. CHO-K1 cells were kindly donated by the Pasteur Institute (Brussels, Belgium).

Cell Culture, Transient Transfection, and Membrane Preparation. CHO-K1 and HEK293 cell lines were cultured in 75 and 500 cm^2 culture flasks in Dulbecco's modified essential medium (DMEM) supplemented with L-glutamine (2 mM), 2% (v/v) of a stock solution containing 5000 IU/mL penicillin and 5000 μg/mL streptomycin (Invitrogen, Merelbeke, Belgium), 1% (v/v) of a stock solution containing nonessential amino acids, 1 mM sodium pyruvate, and 10% (v/v) fetal bovine serum (Invitrogen, Merelbeke, Belgium). The cells were grown in 5% CO_2 at 37 °C until confluence was reached.

HEK293 cells were transiently transfected with plasmid DNA, pCIneo containing the gene of human IRAP (kindly provided by Prof. M. Tsujimoto, Laboratory of Cellular Biochemistry, Saitama, Japan) or pTEJ4[82] carrying the complete human AP-N cDNA.[24] The transient transfection was performed as described previously with 8 μL/mL Lipofectamine (Invitrogen, Merelbeke, Belgium) and 1 μg/mL plasmid DNA.[83] After transfection, the cells were cultured for 2 more days. IRAP and AP-N transfected HEK293 cells displayed 10 and 8 times higher enzyme activity, respectively, than nontransfected cells.

CHO-K1 cell and transfected HEK293 cell membranes were prepared as described previously.[84] Briefly, the cells were harvested with 0.2% 2-[2-[bis(carboxymethyl)amino]ethyl(carboxymethyl)amino]acetic acid (EDTA) (w/v) (in phosphate-buffered saline (PBS), pH 7.4) and centrifuged for 5 min at 500g at room temperature. After resuspension in PBS, the number of cells were counted and washed. The cells were then homogenized in 50 mM Tris-HCl (at pH 7.4) using a Polytron homogenizer (10 s at maximum speed) and a Potter homogenizer (30 strokes at 1000 rpm) and then centrifuged for 30 min (30000g at 4 °C). The pellet was resuspended in 50 mM Tris-HCl, centrifuged (30 min at 30000g at 4 °C), and the supernatant was removed. The resulting pellets were stored at −20 °C until used.

Enzyme Assay. Determination of the aminopeptidase catalytic activity was based on the cleavage of the substrate L-leucine-*p*-nitroanilide (L-Leu-pNA)[84] to give L-leucine and *p*-nitroaniline. This latter compound displays a characteristic light absorption maximum at 405 nm. Pellets, prepared as described above, were thawed and resuspended, using a Polytron homogenizer, in enzyme assay buffer containing 50 mM Tris-HCl (pH 7.4), 140 mM NaCl, 0.1% (w/v) bovine serum albumin (BSA), and 100 μM phenylmethylsulfonyl fluoride (PMSF). The incubation mixture

comprised 50 μL of membrane homogenate, 200 μL of L-Leu-pNA (1.5 mM), and 50 μL of enzyme assay buffer alone or with the test compound. The amount of membrane homogenate corresponded to 1.5×10^5 transfected HEK293 cells in each well. Assays were carried out at 37 °C in 96-well plates (Medisch Labo Service, Menen, Belgium), and the formation of *p*-nitroaniline was followed by measuring the absorption at 405 nm every 5 min between 10 and 50 min in a Tecan M200 96-well reader. The enzymatic activities were calculated by linear regression analysis of the timewise increase in absorption.

Stability Experiments. The stability of the compounds was studied in the presence of CHO-K1 cell membranes. Membrane pellets were thawed and resuspended using a Polytron homogenizer in 50 mM Tris-HCl (pH 7.4) enzyme assay buffer. Preincubation was carried out for 40 min at 37 °C in a finale volume of 250 μL containing 150 μL of membrane homogenate (corresponding to 4×10^5 CHO-K1 cells, 50 μL of enzyme assay buffer without or with 30 mM EDTA/600 μM 1,10-phenantroline (1,10-Phe), and 50 μL of enzyme assay buffer without or with the different compounds or unlabeled Ang IV (60 μM for nonspecific binding). The binding assay was then initiated by adding 50 μL of enzyme assay buffer containing [^{3}H]AL-11 (18 nM, without (if chelators were already present in the preincubation medium) or with 30 mM EDTA/600 μM 1,10-Phe), and the mixture was further incubated for 30 min at 37 °C. The final chelator concentrations were 5 mM EDTA and 100 μM 1,10-Phe. The [^{3}H]AL-11 concentration was 3 nM, and the final unlabeled ligand concentrations ranged from 10^{-5} to 10^{-9} M. After incubation, the mixture was vacuum-filtered using an Inotech 24-well cell harvester through GF/B glass fiber filters (Whatman) presoaked in 1% (w/v) BSA. After drying, the radioactivity retained by the filters was measured (after adding 3 mL of scintillation liquid (Optiphase Hisafe)) using a β-counter (Perkin-Elmer). [^{3}H]AL-11 was characterized as described in Demaegdt et al., 2009.

Data Analysis. All experiments were performed at least twice with duplicate determinations in each experiment. The calculation of IC_{50} values from competition binding (or enzyme inhibition) experiments was performed by nonlinear regression analysis using GraphPad Prism 5.0. The equilibrium dissociation constants (K_i values) of the tested compounds in the binding and enzyme assays were calculated using the equation $K_i = [IC_{50}/(1 + [L]/K)]$ in which [L] is the concentration of the free radioligand (binding) or free substrate concentration (enzyme assay) and K is the equilibrium dissociation constant (KD) of [^{3}H]AL-11 (from saturation binding experiments) or the Michaelis−Menten constant (K_m) for substrate cleavage.[85]

Acknowledgment. We gratefully acknowledge The Swedish Research Council for economic support and the Swedish NMR Centre (SNC) at the University of Gothenburg for a generous allotment of spectrometer time. H.D. is a postdoctoral researcher of the "Fund for Scientific Research—Flanders" (FWO, Belgium). We are grateful to Prof. D. Tourwé and A. Lukaszuk (Department of Organic Chemistry, Vrije Universiteit Brussel, Belgium) for the preparation of the AL-11 precursor and to G. Tóth and E. Szemenyei (Biological Research Center, Szeged, Hungary) for the tritiation of this precursor to [^{3}H]AL-11.[63] We also thank Aleh Yahorau for conducting the HRMS experiments and Henrik Schüller for the development of a tool for computer-aided interproton distance calculations from NOESY data.

Supporting Information Available: Additional synthetic and analytical data, LC−UV and ^{1}H NMR spectroscopy data used in the identification of the isomers of LLL-configuration and the corresponding epimers, and results from the configurational analysis employing the NAMFIS methodology. This material is available free of charge via the Internet at http://pubs.acs.org.

References

(1) Brookmeyer, R.; Johnson, E.; Ziegler-Graham, K.; Arrighi, H. M. Forecasting the global burden of Alzheimer's disease. *Alzheimer's Dementia* **2007**, *3*, 186–191.
(2) Small, G. W.; Rabins, P. V.; Barry, P. P.; Buckholtz, N. S.; DeKosky, S. T.; Ferris, S. H.; Finkel, S. I.; Gwyther, L. P.; Khachaturian, Z. S.; Lebowitz, B. D.; McRae, T. D.; Morris, J. C.; Oakley, F.; Schneider, L. S.; Streim, J. E.; Sunderland, T.; Teri, L. A.; Tune, L. E. Diagnosis and treatment of Alzheimer disease and related disorders. Consensus statement of the American Association for Geriatric Psychiatry, the Alzheimer's Association, and the American Geriatrics Society. *JAMA, J. Am. Med. Assoc.* **1997**, *278*, 1363–1371.
(3) Miguel-Hidalgo, J. J.; Alvarez, X. A.; Cacabelos, R.; Quack, G. Neuroprotection by memantine against neurodegeneration induced by beta-amyloid(1−40). *Brain Res.* **2002**, *958*, 210–221.
(4) Birks, J. Cholinesterase inhibitors for Alzheimer's disease. *Cochrane Database Syst. Rev.* **2006**, CD005593.
(5) Cosman, K. M.; Boyle, L. L.; Porsteinsson, A. P. Memantine in the treatment of mild-to-moderate Alzheimer's disease. *Expert Opin. Pharmacother.* **2007**, *8*, 203–214.
(6) Doraiswamy, P. M.; Xiong, G. L. Pharmacological strategies for the prevention of Alzheimer's disease. *Expert Opin. Pharmacother.* **2006**, *7*, 1–10.
(7) Raina, P.; Santaguida, P.; Ismaila, A.; Patterson, C.; Cowan, D.; Levine, M.; Booker, L.; Oremus, M. Effectiveness of cholinesterase inhibitors and memantine for treating dementia: evidence review for a clinical practice guideline. *Ann. Intern. Med.* **2008**, *148*, 379–397.
(8) Ruther, E.; Ritter, R.; Apecechea, M.; Freytag, S.; Gmeinbauer, R.; Windisch, M. Sustained improvements in patients with dementia of Alzheimer's type (DAT) 6 months after termination of Cerebrolysin therapy. *J. Neural Transm.* **2000**, *107*, 815–829.
(9) Nunomura, A.; Perry, G.; Smith, M. A. Prospects for Antioxidant Therapy in Mild Cognitive Impairment and Alzheimer'S Disease. In *Oxidative Stress and Neurodegenerative Disorders*; Qureshi, G. A., Parvez, S. H., Eds.; Elsevier B.V.: Amsterdam, 2007; pp 451−466.
(10) Sonnen, J. A.; Breitner, J. C.; Lovell, M. A.; Markesbery, W. R.; Quinn, J. F.; Montine, T. J. Free radical-mediated damage to brain in Alzheimer's disease and its transgenic mouse models. *Free Radical Biol. Med.* **2008**, *45*, 219–230.
(11) Lonn, E.; Bosch, J.; Yusuf, S.; Sheridan, P.; Pogue, J.; Arnold, J. M.; Ross, C.; Arnold, A.; Sleight, P.; Probstfield, J.; Dagenais, G. R. Effects of long-term vitamin E supplementation on cardiovascular events and cancer: a randomized controlled trial. *JAMA, J. Am. Med. Assoc.* **2005**, *293*, 1338–1347.
(12) Salloway, S.; Mintzer, J.; Weiner, M. F.; Cummings, J. L. Disease-modifying therapies in Alzheimer's disease. *Alzheimer's Dementia* **2008**, *4*, 65–79.
(13) Upton, N.; Chuang, T. T.; Hunter, A. J.; Virley, D. J. 5-HT_6 receptor antagonists as novel cognitive enhancing agents for Alzheimer's disease. *Neurotherapeutics* **2008**, *5*, 458–469.
(14) Wolfe, M. S. Therapeutic strategies for Alzheimer's disease. *Nat. Rev. Drug Discovery* **2002**, *1*, 859–866.
(15) Wright, J. W.; Harding, J. W. The angiotensin AT_4 receptor subtype as a target for the treatment of memory dysfunction associated with Alzheimer's disease. *J. Renin−Angiotensin−Aldosterone Syst.* **2008**, *9*, 226–237.
(16) Braszko, J. J.; Kupryszewski, G.; Witczuk, B.; Wisniewski, K. Angiotensin II-(3−8)-hexapeptide affects motor activity, performance of passive avoidance and a conditioned avoidance response in rats. *Neuroscience* **1988**, *27*, 777–783.
(17) Braszko, J. J.; Wlasienko, J.; Koziolkiewicz, W.; Janecka, A.; Wisniewski, K. The 3−7 fragment of angiotensin II is probably responsible for its psychoactive properties. *Brain Res.* **1991**, *542*, 49–54.
(18) Chai, S. Y.; Yeatman, H. R.; Parker, M. W.; Ascher, D. B.; Thompson, P. E.; Mulvey, H. T.; Albiston, A. L. Development of cognitive enhancers based on inhibition of insulin-regulated aminopeptidase. *BMC Neurosci.* **2008**, *9* (Suppl. 2), S14.
(19) Hallberg, M. Targeting the insulin-regulated aminopeptidase/AT_4 receptor for cognitive disorders. *Drug News Perspect.* **2009**, *22*, 133–139.
(20) Albiston, A. L.; McDowall, S. G.; Matsacos, D.; Sim, P.; Clune, E.; Mustafa, T.; Lee, J.; Mendelsohn, F. A.; Simpson, R. J.; Connolly, L. M.; Chai, S. Y. Evidence that the angiotensin IV (AT(4)) receptor is the enzyme insulin-regulated aminopeptidase. *J. Biol. Chem.* **2001**, *276*, 48623–48626.
(21) Chai, S. Y.; Bastias, M. A.; Clune, E. F.; Matsacos, D. J.; Mustafa, T.; Lee, J. H.; McDowall, S. G.; Paxinos, G.; Mendelsohn, F. A.;

Albiston, A. L. Distribution of angiotensin IV binding sites (AT_4 receptor) in the human forebrain, midbrain and pons as visualised by in vitro receptor autoradiography. *J. Chem. Neuroanat.* **2000**, *20*, 339–348.
(22) Fernando, R. N.; Larm, J.; Albiston, A. L.; Chai, S. Y. Distribution and cellular localization of insulin-regulated aminopeptidase in the rat central nervous system. *J. Comp. Neurol.* **2005**, *487*, 372–390.
(23) Moeller, I.; Paxinos, G.; Mendelsohn, F. A.; Aldred, G. P.; Casley, D.; Chai, S. Y. Distribution of AT_4 receptors in the *Macaca fascicularis* brain. *Brain Res.* **1996**, *712*, 307–324.
(24) Olsen, J.; Cowell, G. M.; Konigshofer, E.; Danielsen, E. M.; Moller, J.; Laustsen, L.; Hansen, O. C.; Welinder, K. G.; Engberg, J.; Hunziker, W. Complete amino acid sequence of human intestinal aminopeptidase N as deduced from cloned cDNA. *FEBS Lett.* **1988**, *238*, 307–314.
(25) Keller, S. R.; Scott, H. M.; Mastick, C. C.; Aebersold, R.; Lienhard, G. E. Cloning and characterization of a novel insulin-regulated membrane aminopeptidase from Glut4 vesicles. *J. Biol. Chem.* **1995**, *270*, 23612–23618.
(26) Lukaszuk, A.; Demaegdt, H.; Feytens, D.; Vanderheyden, P.; Vauquelin, G.; Tourwe, D. The replacement of His^4 in angiotensin IV by conformationally constrained residues provides highly potent and selective analogues. *J. Med. Chem.* **2009**, *52*, 5612–5618.
(27) Lukaszuk, A.; Demaegdt, H.; Szemenyei, E.; Toth, G.; Tymecka, D.; Misicka, A.; Karoyan, P.; Vanderheyden, P.; Vauquelin, G.; Tourwe, D. Beta-Homo-amino acid scan of angiotensin IV. *J. Med. Chem.* **2008**, *51*, 2291–2296.
(28) Albiston, A. L.; Morton, C. J.; Ng, H. L.; Pham, V.; Yeatman, H. R.; Ye, S.; Fernando, R. N.; De Bundel, D.; Ascher, D. B.; Mendelsohn, F. A.; Parker, M. W.; Chai, S. Y. Identification and characterization of a new cognitive enhancer based on inhibition of insulin-regulated aminopeptidase. *FASEB J.* **2008**, *22*, 4209–4217.
(29) Andersson, H.; Demaegdt, H.; Vauquelin, G.; Lindeberg, G.; Karlen, A.; Hallberg, M. Ligands to the (IRAP)/AT_4 receptor encompassing a 4-hydroxydiphenylmethane scaffold replacing Tyr2. *Bioorg. Med. Chem.* **2008**, *16*, 6924–6935.
(30) Axén, A.; Andersson, H.; Lindeberg, G.; Ronnholm, H.; Kortesmaa, J.; Demaegdt, H.; Vauquelin, G.; Karlen, A.; Hallberg, M. Small potent ligands to the insulin-regulated aminopeptidase (IRAP)/AT_4 receptor. *J. Pept. Sci.* **2007**, *13*, 434–444.
(31) Axén, A.; Lindeberg, G.; Demaegdt, H.; Vauquelin, G.; Karlén, A.; Hallberg, M. Cyclic insulin-regulated aminopeptidase (IRAP)/AT_4 receptor ligands. *J. Pept. Sci.* **2006**, *12*, 705–713.
(32) Carpino, L. A.; Han, G. Y. 9-Fluorenylmethoxycarbonyl amino-protecting group. *J. Org. Chem.* **1972**, *37*, 3404–3409.
(33) Angell, Y. M.; Alsina, J.; Albericio, F.; Barany, G. Practical protocols for stepwise solid-phase synthesis of cysteine-containing peptides. *J. Pept. Res.* **2002**, *60*, 292–299.
(34) Wallace, T. J.; Mahon, J. J. Reactions of thiols with sulfoxides. II. Kinetics and mechanistic implications. *J. Am. Chem. Soc.* **2002**, *86*, 4099–4103.
(35) Otaka, A.; Koide, T.; Shide, A.; Fujii, N. Application of dimethylsulphoxide(DMSO)/trifluoroacetic acid(TFA) oxidation to the synthesis of cystine-containing peptide. *Tetrahedron Lett.* **1991**, *32*, 1223–1226.
(36) Tam, J. P.; Wu, C. R.; Liu, W.; Zhang, J. W. Disulfide bond formation in peptides by dimethyl sulfoxide. Scope and applications. *J. Am. Chem. Soc.* **2002**, *113*, 6657–6662.
(37) Tang, Z. L.; Pelletier, J. C. Preparation of amides from acids and resin bound azides: suppression of intramolecular lactam formation. *Tetrahedron Lett.* **1998**, *39*, 4773–4776.
(38) Brandt, M.; Gammeltoft, S.; Jensen, K. Microwave heating for solid-phase peptide synthesis: general evaluation and application to 15-mer phosphopeptides. *Int. J. Pept. Res. Ther.* **2006**, *12*, 349–357.
(39) Vázquez, J.; Albericio, F. A useful and sensitive color test to monitor aldehydes on solid-phase. *Tetrahedron Lett.* **2001**, *42*, 6691–6693.
(40) Kay, C.; Lorthioir, O. E.; Parr, N. J.; Congreve, M.; McKeown, S. C.; Scicinski, J. J.; Ley, S. V. Solid-phase reaction monitoring—chemical derivatization and off-bead analysis. *Biotechnol. Bioeng.* **2000**, *71*, 110–118.
(41) Vojkovsky, T. Detection of secondary amines on solid phase. *Pept. Res.* **1995**, *8*, 236–237.
(42) Nevins, N.; Cicero, D.; Snyder, J. P. A test of the single-conformation hypothesis in the analysis of NMR data for small polar molecules: a force field comparison. *J. Org. Chem.* **1999**, *64*, 3979–3986.
(43) Beckers, M. L.; Buydens, L. M.; Pikkemaat, J. A.; Altona, C. Application of a genetic algorithm in the conformational analysis of methylene-acetal-linked thymine dimers in DNA: comparison with distance geometry calculations. *J. Biomol. NMR* **1997**, *9*, 25–34.
(44) Blackledge, M. J.; Bruschweiler, R.; Griesinger, C.; Schmidt, J. M.; Xu, P.; Ernst, R. R. Conformational backbone dynamics of the cyclic decapeptide antamanide. Application of a new multiconformational search algorithm based on NMR data. *Biochemistry* **1993**, *32*, 10960–10974.
(45) Bruschweiler, R.; Blackledge, M.; Ernst, R. R. Multi-conformational peptide dynamics derived from NMR data: a new search algorithm and its application to antamanide. *J. Biomol. NMR* **1991**, *1*, 3–11.
(46) Landis, C.; Allured, V. S. Elucidation of solution structures by conformer population analysis of NOE data. *J. Am. Chem. Soc.* **1991**, *113*, 9493–9499.
(47) Cicero, D. O.; Barbato, G.; Bazzo, R. NMR analysis of molecular flexibility in solution: a new method for the study of complex distributions of rapidly exchanging conformations. Application to a 13-residue peptide with an 8-residue loop. *J. Am. Chem. Soc.* **1995**, *117*, 1027–1033.
(48) Pearlman, D. A. FINGAR, a new genetic algorithm-based method for fitting NMR data. *J. Biomol. NMR* **1996**, *8*, 49–66.
(49) Wang, J.; Hodges, R. S.; Sykes, B. D. Generating multiple conformations of flexible peptides in solution on the basis of NMR nuclear Overhauser effect data: application to desmopressin. *J. Am. Chem. Soc.* **1995**, *117*, 8627–8634.
(50) Thepchatri, P.; Cicero, D. O.; Monteagudo, E.; Ghosh, A. K.; Cornett, B.; Weeks, E. R.; Snyder, J. P. Conformations of laulimalide in DMSO-d_6. *J. Am. Chem. Soc.* **2005**, *127*, 12838–12846.
(51) Bifulco, G.; Dambruoso, P.; Gomez-Paloma, L.; Riccio, R. Determination of relative configuration in organic compounds by NMR spectroscopy and computational methods. *Chem. Rev.* **2007**, *107*, 3744–3779.
(52) Matsumori, N.; Kaneno, D.; Murata, M.; Nakamura, H.; Tachibana, K. Stereochemical determination of acyclic structures based on carbon-proton spin-coupling constants. A method of configuration analysis for natural products. *J. Org. Chem.* **1999**, *64*, 866–876.
(53) Farès, C.; Hassfeld, J.; Menche, D.; Carlomagno, T. Simultaneous determination of the conformation and relative configuration of archazolide A by using nuclear Overhauser effects, *J* couplings, and residual dipolar couplings. *Angew. Chem., Int. Ed.* **2008**, *47*, 3722–3726.
(54) Sanchez-Pedregal, V. M.; Santamaria-Fernandez, R.; Navarro-Vazquez, A. Residual dipolar couplings of freely rotating groups in small molecules. Stereochemical assignment and side-chain conformation of 8-phenylmenthol. *Org. Lett.* **2009**, *11*, 1471–1474.
(55) Thiele, C. M. Simultaneous assignment of all diastereotopic protons in strychnine using RDCs: PELG as alignment medium for organic molecules. *J. Org. Chem.* **2004**, *69*, 7403–7413.
(56) Thiele, C. M. Residual dipolar couplings (RDCs) in organic structure determination. *Eur. J. Org. Chem.* **2008**, 5673–5685.
(57) Demaegdt, H.; Laeremans, H.; De Backer, J.-P.; Mosselmans, S.; Le, M. T.; Kersemans, V.; Michotte, Y.; Vauquelin, G.; Vanderheyden, P. M. L. Synergistic modulation of cystinyl aminopeptidase by divalent cation chelators. *Biochem. Parmacol.* **2004**, *68*, 893–900.
(58) Demaegdt, H.; Lenaerts, P. J.; Swales, J.; De Backer, J. P.; Laeremans, H.; Le, M. T.; Kersemans, K.; Vogel, L. K.; Michotte, Y.; Vanderheyden, P.; Vauquelin, G. Angiotensin AT_4 receptor ligand interaction with cystinyl aminopeptidase and aminopeptidase N: [^{125}I]angiotensin IV only binds to the cystinyl aminopeptidase apoenzyme. *Eur. J. Pharmacol.* **2006**, *546*, 19–27.
(59) Kobori, T.; Goda, K.; Sugimoto, K.; Ota, T.; Tomisawa, K. Preparation of Peptide Derivatives as Angiotensin IV Receptor Agonists. WO 97/03093 A1, 1997.
(60) Kobori, T.; Goda, K.; Sugimoto, K.; Ota, T.; Tomisawa, K. Preparation of Amino Acid Derivatives as Angiotensin IV Receptor Agonists. WO 98/05624 A1, 1998.
(61) Sardinia, M. F.; Hanesworth, J. M.; Krebs, L. T.; Harding, J. W. AT_4 receptor binding characteristics: D-amino acid- and glycine-substituted peptides. *Peptides* **1993**, *14*, 949–954.
(62) Sardinia, M. F.; Hanesworth, J. M.; Krishnan, F.; Harding, J. W. AT_4 receptor structure−binding relationship: N-terminal-modified angiotensin IV analogues. *Peptides* **1994**, *15*, 1399–1406.
(63) Demaegdt, H.; Lukaszuk, A.; De Buyser, E.; De Backer, J. P.; Szemenyei, E.; Toth, G.; Chakravarthy, S.; Panicker, M.; Michotte, Y.; Tourwe, D.; Vauquelin, G. Selective labeling of IRAP by the tritiated AT_4 receptor ligand [^{3}H]angiotensin IV and its stable analog [^{3}H]AL-11. *Mol. Cell. Endocrinol.* **2009**, *311*, 77–86.
(64) Demaegdt, H.; Laeremans, H.; De Backer, J. P.; Mosselmans, S.; Le, M. T.; Kersemans, V.; Michotte, Y.; Vauquelin, G.; Vanderheyden, P. M. Synergistic modulation of cystinyl aminopeptidase by divalent cation chelators. *Biochem. Pharmacol.* **2004**, *68*, 893–900.

(65) Kenny, A. J. Regulatory peptide metabolism at cell surfaces: the key role of endopeptidase-24.11. *Biomed. Biochim. Acta* **1986**, *45*, 1503–1513.
(66) Lalu, K.; Lampelo, S.; Vanha-Perttula, T. Characterization of three aminopeptidases purified from maternal serum. *Biochim. Biophys. Acta* **1986**, *873*, 190–197.
(67) Laustsen, P. G.; Vang, S.; Kristensen, T. Mutational analysis of the active site of human insulin-regulated aminopeptidase. *Eur. J. Biochem.* **2001**, *268*, 98–104.
(68) Schmidt, B.; Lindman, S.; Tong, W.; Lindeberg, G.; Gogoll, A.; Lai, Z.; Thornwall, M.; Synnergren, B.; Nilsson, A.; Welch, C. J.; Sohtell, M.; Westerlund, C.; Nyberg, F.; Karlen, A.; Hallberg, A. Design, synthesis, and biological activities of four angiotensin II receptor ligands with gamma-turn mimetics replacing amino acid residues 3−5. *J. Med. Chem.* **1997**, *40*, 903–919.
(69) Sigel, H.; Martin, R. B. Coordinating properties of the amide bond. Stability and structure of metal ion complexes of peptides and related ligands. *Chem. Rev.* **1982**, *82*, 385–426.
(70) Ye, S.; Chai, S. Y.; Lew, R. A.; Ascher, D. B.; Morton, C. J.; Parker, M. W.; Albiston, A. L. Identification of modulating residues defining the catalytic cleft of insulin-regulated aminopeptidase. *Biochem. Cell Biol.* **2008**, *86*, 251–261.
(71) Tholander, F.; Muroya, A.; Roques, B. P.; Fournie-Zaluski, M. C.; Thunnissen, M. M.; Haeggstrom, J. Z. Structure-based dissection of the active site chemistry of leukotriene A4 hydrolase: implications for M1 aminopeptidases and inhibitor design. *Chem. Biol.* **2008**, *15*, 920–929.
(72) Ito, K.; Nakajima, Y.; Onohara, Y.; Takeo, M.; Nakashima, K.; Matsubara, F.; Ito, T.; Yoshimoto, T. Crystal structure of aminopeptidase N (proteobacteria alanyl aminopeptidase) from *Escherichia coli* and conformational change of methionine 260 involved in substrate recognition. *J. Biol. Chem.* **2006**, *281*, 33664–33676.
(73) Ye, S.; Chai, S. Y.; Lew, R. A.; Albiston, A. L. Insulin-regulated aminopeptidase: analysis of peptide substrate and inhibitor binding to the catalytic domain. *Biol. Chem.* **2007**, *388*, 399–403.
(74) Bodenhausen, G.; Wagner, G.; Rance, M.; Sorensen, O. W.; Wuthrich, K.; Ernst, R. R. Longitudinal 2-spin order in 2D exchange spectroscopy (NOESY). *J. Magn. Reson.* **1984**, *59*, 542–550.
(75) Meier, B. H.; Ernst, R. R. Elucidation of chemical exchange networks by two-dimensional NMR spectroscopy: the heptamethylbenzenonium ion. *J. Am. Chem. Soc.* **1979**, *101*, 6441–6442.
(76) Griesinger, C.; Sørensen, O. W.; Ernst, R. R. Practical aspects of the E.COSY technique. Measurement of scalar spin−spin coupling constants in peptides. *J. Magn. Reson.* **1987**, *75*, 474–492.
(77) Mohamadi, F.; Richards, N. G. J.; Guida, W. C.; Liskamp, R.; Lipton, M.; Caufield, C.; Chang, G.; Hendrickson, T.; Still, W. C. Macromodel—an integrated software system for modeling organic and bioorganic molecules using molecular mechanics. *J. Comput. Chem.* **1990**, *11*, 440–467.
(78) Still, W. C.; Tempczyk, A.; Hawley, R. C.; Hendrickson, T. Semianalytical treatment of solvation for molecular mechanics and dynamics. *J. Am. Chem. Soc.* **1990**, *112*, 6127–6129.
(79) Kessler, H.; Griesinger, C.; Lautz, J.; Muller, A.; Vangunsteren, W. F.; Berendsen, H. J. C. Conformational dynamics detected by nuclear magnetic resonance NOE values and *J* coupling constants. *J. Am. Chem. Soc.* **1988**, *110*, 3393–3396.
(80) Schmidt, J. M. A versatile component-coupling model to account for substituent effects: Application to polypeptide ϕ and χ_1 torsion related ^3J data. *J. Magn. Reson.* **2007**, *186*, 34–50.
(81) Haasnoot, C. A. G.; Deleeuw, F. A. A. M.; Altona, C. The relationship between proton−proton NMR coupling-constants and substituent electronegativities—I. An empirical generalization of the Karplus equation. *Tetrahedron* **1980**, *36*, 2783–2792.
(82) Johansen, T. E.; Scholler, M. S.; Tolstoy, S.; Schwartz, T. W. Biosynthesis of peptide precursors and protease inhibitors using new constitutive and inducible eukaryotic expression vectors. *FEBS Lett.* **1990**, *267*, 289–294.
(83) Le, M. T.; De Backer, J. P.; Hunyady, L.; Vanderheyden, P. M.; Vauquelin, G. Ligand binding and functional properties of human angiotensin AT_1 receptors in transiently and stably expressed CHO-K1 cells. *Eur. J. Pharmacol.* **2005**, *513*, 35–45.
(84) Demaegdt, H.; Vanderheyden, P.; De Backer, J. P.; Mosselmans, S.; Laeremans, H.; Le, M. T.; Kersemans, V.; Michotte, Y.; Vauquelin, G. Endogenous cystinyl aminopeptidase in Chinese hamster ovary cells: characterization by [^{125}I]Ang IV binding and catalytic activity. *Biochem. Pharmacol.* **2004**, *68*, 885–892.
(85) Cheng, Y.; Prusoff, W. H. Relationship between the inhibition constant (K_i) and the concentration of inhibitor which causes 50% inhibition (IC_{50}) of an enzymatic reaction. *Biochem. Pharmacol.* **1973**, *22*, 3099–3108.
(86) The difference in the magnitude of the SSD values for **12** and **13** originates from the nature of the SSD. Its absolute value depends on the number of used constraints.[42]